Analytical modeling of degradation product partitioning kinetics in source zones containing entrapped DNAPL

C. Andrew Ramsburg,[1] John A. Christ,[2] Scott R. Douglas,[3] and Ali Boroumand[1]

Received 30 August 2010; revised 16 November 2010; accepted 28 December 2010; published 2 March 2011.

[1] Liquid-liquid equilibrium experiments indicate that there is a strong thermodynamic driving force for the reversible sequestration of *cis*-dichloroethene (DCE) within microbially active dense nonaqueous phase liquid (DNAPL) source zones containing chlorinated ethene solvents. Assessment of the importance of degradation product sequestration, however, requires accurate description of the mass transfer kinetics. Partitioning kinetics of *cis*-DCE were assessed in a series of transport experiments conducted in sandy columns containing uniformly entrapped tetrachloroethene (PCE)-nonaqueous phase liquids (NAPL). Effluent data from these experiments were simulated using an analytical solution adapted from the sorption literature. The solution permits interrogation of the relative importance of mass transfer resistance in the aqueous phase and NAPL. Column data and simulations suggest that the kinetic exchange of *cis*-DCE may be described with mass transfer correlations developed for the dissolution of pure component NAPLs. Diffusive transport within the entrapped ganglia was relatively fast, offering limited resistance to mass exchange. These results (1) establish the applicability of dissolution-based mass transfer correlations for modeling both absorption and dissolution of degradation products, (2) quantify the thermodynamic driving force for the partitioning of *cis*-DCE in PCE-NAPL by assessing the ternary phase behavior, and (3) guide incorporation and deployment of partitioning kinetics into multiphase compositional simulators when assessing or designing metabolic reductive dechlorination within DNAPL source zones. While focus is placed on examining degradation product partitioning in DNAPL source zones, results may also be useful when considering rate limitations in other liquid-liquid partitioning processes, such as partitioning tracer tests.

Citation: Ramsburg, C. A., J. A. Christ, S. R. Douglas, and A. Boroumand (2011), Analytical modeling of degradation product partitioning kinetics in source zones containing entrapped DNAPL, *Water Resour. Res., 47*, W03507, doi:10.1029/2010WR009958.

1. Introduction

[2] The quantification of liquid-liquid partitioning in contaminated subsurface environments is essential when attempting to describe the fate and transport of degradation products within nonaqueous phase liquid (NAPL) source zones. Sequestration of degradation products in immobile NAPL is often proposed as a physical-chemical mechanism influencing contaminant bioavailability and, hence, degradation rates and long-term remediation success [*Carr et al.*, 2000; *Cope and Hughes*, 2001; *Yang and McCarty*, 2002; *Adamson et al.*, 2004, *Amos et al.*, 2007; *Christ and Abriola*, 2007; *Ramsburg et al.*, 2010]. Despite its importance, however, little work has focused on the kinetics of degradation product partitioning in subsurface NAPL source zones.

[3] Consideration of liquid-liquid partitioning in NAPL source zones has generally been associated with partitioning interwell trace tests (PITT), which inject partitioning and nonpartitioning tracers through a zone contaminated with immobile NAPL to quantify subsurface saturations [e.g., *Jin et al.*, 1995; *Annable et al.*, 1998]. The first descriptions of kinetic, liquid-liquid partitioning in the subsurface were based upon two-region models where exchange occurred between a mobile (flowing) aqueous phase and immobile (stagnant) aqueous phase, as might be found in the dead-end pores of soil grains [*van Genuchten and Wierenga*, 1976, 1977; *van Genuchten et al.*, 1977; *Rao et al.*, 1980; *Nkedi-Kizza et al.*, 1982; *Hatfield and Stauffer*, 1993]. Two-region partitioning has been modeled using a linear driving force expression, assuming partitioning to the immobile aqueous phase is controlled by mass transfer across a thin film boundary layer [e.g., *van Genuchten and Wierenga*, 1976; *van Genuchten and Wagenet*, 1989; *Toride et al.*, 1993, 1999] or by solving a second equation that describes diffusion within the immobile aqueous phase as the process controlling partitioning kinetics [*Rao et al.*, 1980; *Rasmuson and Neretnieks*, 1980, 1981; *Huang et al.*, 1984; *van Genuchten*, 1985; *Crittenden et al.*, 1986; *Carta and Bauer*, 1990; *Willson et al.*, 2000; *Li et al.*, 2003]. These governing equations have been solved analytically

[1]Department of Civil and Environmental Engineering, Tufts University, Medford, Massachusetts, USA.
[2]Department of Civil and Environmental Engineering, United States Air Force Academy, Colorado Springs, Colorado, USA.
[3]Geosyntec Consultants, Lawrenceville, New Jersey, USA.

0043-1397/11/2010WR009958

and numerically and continue to serve as a foundation for investigating subsurface contaminant transport.

[4] Few studies, however, have investigated the influence of partitioning kinetics on degradation product fate and transport in NAPL source zones, perhaps because of the uncertainty regarding parameterization of the model and mass exchange kinetics or the elucidation of the thermodynamic driving force [*Hatfield and Stauffer*, 1993]. Liquid-liquid partitioning is especially important in chlorinated dense nonaqueous phase liquid (DNAPL) source zones where the DNAPL serves as a persistent source of contaminant (e.g., tetrachloroethene (PCE)) mass and the one-to-one stoichiometry of the transformation process often leads to near mM concentrations of degradation products (e.g., *cis*-1,2-dichloroethene (*cis*-DCE)) [*Carr et al.*, 2000; *Yang and McCarty*, 2000; *Adamson et al.*, 2004; *Amos et al.*, 2008; *Interstate Technology and Regulatory Council*, 2008; *Yu and Semprini*, 2009]. The production of degradation products in the aqueous phase provides a strong driving force for degradation product partitioning into the immobile DNAPL. This partitioning process serves to reversibly sequester the degradation product mass. Reversible sequestration can lead to (1) an underestimation of degradation kinetics by neglecting product mass within the NAPL, and (2) retardation of degradation product transport because of partitioning between the NAPL and aqueous phases (analogous to liquid-solid sorption). Recently quantified partition coefficients for two of the most common degradation product-DNAPL combinations, *cis*-DCE in PCE-DNAPL and vinyl chloride (VC) in trichloroethene (TCE)-DNAPL demonstrate that even moderate DNAPL saturations (e.g., 2%), can sequester 60 to 70% of the degradation product mass [*Ramsburg et al.*, 2010]. The results of *Ramsburg et al.* [2010], which elucidate the equilibrium partitioning behavior at low concentration, motivate further study to quantify partitioning at higher concentration and to quantify partitioning kinetics under conditions of nonequilibrium transport. The latter is particularly important given that Ramsburg et al. included an illustrative simulation to assess possible implications of kinetic partitioning of degradation products produced within a bioactive DNAPL source zone. This simulation approximated the absorption rate of *cis*-DCE at low concentration with the mass transfer rate produced from a correlation developed for NAPL dissolution [e.g., *Powers et al.*, 1992]. Diffusion within the NAPL may, however, limit the exchange process [*Willson et al.*, 2000]. Thus, use of dissolution-based correlations for mass transfer [e.g., *Miller et al.*, 1990; *Imhoff et al.*, 1994; *Powers et al.*, 1992, 1994a] represents a simplification that requires verification prior to widespread integration into multiphase compositional simulators.

[5] The research described herein combined experiments and simulations conducted at the batch and column scale to elucidate the extent and kinetics of *cis*-DCE partitioning between an aqueous phase and a uniformly entrapped PCE-NAPL. Universal functional activity coefficient (UNIFAC) predictions of the phase behavior and phase distribution of *cis*-DCE were compared to experimentally obtained phase data. Models developed to assess the influence of sorption (soils) on contaminant transport were adapted to describe liquid-liquid partitioning in chlorinated DNAPL source zones [*Rasmuson and Neretnieks*, 1980]. Data, simulations, and sensitivity analyses were employed to assess limitations when modeling degradation products partitioning to (and from) entrapped DNAPL using mass transfer correlations developed for NAPL dissolution.

2. Materials and Methods

2.1. Materials

[6] Tetrachloroethene (PCE, 99% purity, ACS grade) and *cis*-1,2-dichlorotethene (*cis*-DCE, 97% purity) were purchased from Sigma-Aldrich Inc. Acetonitrile (99.9% purity, ACS high-performance liquid chromatography (HPLC) grade), dimethyl sulfoxide (DMSO, 99.9% purity), methanol (99.9% purity, ACS HPLC grade), sodium bromide (NaBr, 99.9% purity, ACS grade), and sodium chloride (NaCl, 100% purity, ACS grade) were obtained from Fisher Scientific. Isopropanol (99.9% purity, HPLC grade) was obtained from Acros Organics. All chemicals were used as received. The water used in all batch and column experiments was purified to a resistivity $> 18.1\ M\Omega \times cm$ and total organic carbon (TOC) < 100 ppb using a Milli-Q ultrapure water system (model Gradient A10, Millipore).

[7] Ottawa sands (U.S. Silica Co.) were used to construct porous media employed in the column experiments. ASTM 20–30 mesh sand was used as received, while ASTM 45–50 and ASTM 50–60 mesh sands were produced by sieving Federal Fine sand (ASTM 30–140 mesh). The mean grain size diameter, d_{50}, for the 20–30, 45–50, and 50–60 mesh sands are 725, 328, and 275 μm, respectively. Uniformity indices, $U_i \left(d_{60}/d_{10}\right)$, for these fractions are 1.20, 1.09, and 1.10, respectively.

2.2. Batch Methods

[8] Liquid-liquid equilibrium experiments were conducted in 35 mL glass centrifuge tubes sealed with Teflon-lined screw-on caps following methods similar to those reported by *Ramsburg et al.* [2010]. In brief, tubes were loaded with Milli-Q water, *cis*-DCE, and PCE to arbitrarily predetermined overall mole fractions and allowed to mix on LabQuake oscillating shaker trays at 22.0 ± 0.1 °C for 72 h. Previous experiments have demonstrated 72 h is sufficient time for liquid phase equilibration [*Cope and Hughes*, 2001, *Ramsburg and Pennell*, 2002]. Following the equilibration period, the batch systems were centrifuged at 1500 rpm for 10 min to consolidate each phase prior to separation and sampling. Approximately 5 g of the aqueous phase and 10 μL of the organic phase were diluted (by mass) into a mixture of Milli-Q water and DMSO to fall within the linear response range of the gas chromatographic method (see analytical methods). DMSO was employed as a cosolvent at approximately 11% by weight in all diluted samples.

2.3. Column Methods

[9] Kontes borosilicate glass columns (4.8 cm inner diameter (ID)) were used for all transport experiments. Each column was dry packed with an Ottawa sand fraction (described in section 2.1), flushed with CO_2 for a minimum of 10 pore volumes, and then saturated by flushing Milli-Q water through the column for 20 pore volumes. The PCE used as the DNAPL was dyed red with 1×10^{-4} M of Oil Red O (Alfa Aesar) for visualization within the columns.

PCE-DNAPL entrapment was performed following established methods [*Pennell et al.*, 1993]. Nonreactive, conservative tracer tests were conducted using aqueous solutions of 0.01 M Br^- before and after the introduction of DNAPL to characterize the porous medium employed in each column experiment. Subsequent to the completion of the second tracer test, a pulse (approximately 250 min) of aqueous solution containing approximately 165 mg/L *cis*-DCE was introduced to the column at a rate of 2.0 mL/min using an Agilent Series 1100 quaternary pump. The *cis*-DCE pulses were produced from the column using Milli-Q water delivered at the same rate. The concentrations of *cis*-DCE and PCE in the column effluent were quantified using an inline sampling and analysis system described in section 2.4. Following the cessation of flow, the column was deconstructed and extracted for mass balance purposes.

2.4. Analytical Methods

[10] Batch experiment samples were quantified in triplicate using a Hewlett-Packard 5890 Series II gas chromatograph (GC) equipped with a Perkin Elmer TurboMatrix 40 Trap headspace sampler and flame ionization detector. The GC was calibrated prior to each day of use with a seven-point calibration curve. Headspace vials containing the diluted samples were heated to 95 °C and shaken for 25 min prior to sample transfer to the GC where separation was accomplished on a HP-Plot Q capillary column (30 m length, 0.53 mm ID, 40 μm film thickness).

[11] Column experiments employed an inline sampling system comprising a 10-port, 2-position electric valve (model EHMA, Valco Instruments Co. Inc.) fitted with a 20 μL sample loop. The valve was plumbed in line with: (1) the effluent end of the column; and (2) an Agilent Series 1100 HPLC. The HPLC was equipped with an Agilent Zorbax Eclipse XDB-C8 packed chromatography column (150 mm length, 4.6 mm ID, 5 μm particle diameter) maintained at 40.0 °C and a diode array detector set to quantify absorbance at 254 nm. The HPLC was operated at 1 mL/min under isocratic conditions with mobile phase composition of 80% acetonitrile and 20% Milli-Q water. Under these conditions, the average HPLC column retention times for *cis*-DCE and PCE were approximately 2.3 and 3.2 min, respectively. The HPLC system was calibrated before each day of use using a 6-point standard curve established by introducing standards through a 20 μL sampling valve. The inline system was programmed to sample the column effluent every 4.0 min. At the end of each experiment the contents of the column were extracted with isopropanol to close mass balances. Extract samples were diluted to fall within the range of a 6-point calibration curve, and analyzed using an Agilent Series 1100 autosampler connected to the HPLC. The HPLC method was similar to that employed for effluent sampling but excluded commands for firing the Valco valve.

[12] Effluent samples collected during nonreactive tracer tests were analyzed for bromide and chloride using a Dionex ICS-2000 Ion Chromatograph (IC) equipped with an AS50 autosampler and fitted with an IonPac AS18 anion-exchange column (250 mm length, 4 mm ID, 7.5 μm particle diameter). Isocratic separation was accomplished at 1 mL/min using a mobile phase containing 23.0 mM KOH. Under these conditions, the average retention times for Cl^- and Br^- were approximately 4.4 and 6.8 min, respectively. The IC was calibrated before each day of use using a 6-point standard curve with calibration checks performed every 20 samples.

[13] The densities of the liquid phases present in the batch experiments were quantified in triplicate at 22.0 $\pm$ 0.1 °C using 2 mL glass pycnometers (Ace Glass). Each day of use the pycnometers were calibrated using Milli-Q water. Calibrations were subsequently verified using isopropanol. Water content was quantified using a Karl Fisher titrator (model DL38, Mettler Toledo). The instrument was calibrated with a water standard (1% water by weight, EMD Chemicals, Inc.) on each day of use.

2.5. Thermodynamic Modeling

[14] Ternary phase behavior was predicted using an isothermal flash calculation [*Smith and Van Ness*, 1987] performed in Matlab version R2009b (The MathWorks, Inc.) with UNIFAC [*Fredenslund et al.*, 1975] employed to estimate activity coefficients. Iteration convergence was established when successive changes to molar phase fractions and component mole fractions were less than 1×10^{-10}. No attempt was made to adjust the UNIFAC parameters to fit the data. Structural parameters for the relevant subgroups were obtained from the work of *Hansen et al.* [1991] with water assigned as 1 × H_20 (group 7), *cis*-DCE assigned as 1 × HC=C (group 2) and 2 × Cl-C=C (group 37), and PCE assigned as 1 × C=C (group 2) & 3 × Cl-C=C (group 37). Interaction parameters between groups m and n are $a_{m,n}$ and $a_{n,m}$, both defined in Kelvin, where: $a_{m,m} = a_{n,n} = 0$ (by definition); $a_{2,7} = 785.6$, $a_{7,2} = -26.52$ [*Cooling et al.*, 1992]; $a_{7,37} = 651.9$, $a_{37,7} = 1100$ [*Cooling et al.*, 1992]; and $a_{2,37} = 237.3$ and $a_{37,2} = -3.167$ [*Gmehling et al.*, 1982].

2.6. Mathematical Modeling

[15] Simulation of contaminant transport in the NAPL-contaminated columns was based on the solution of component mass balance equations assuming steady flow and an immobile (entrapped) NAPL saturation [*Abriola*, 1989]. Component mass balance equations solve for the spatial-temporal distribution of a mass concentration of component i (C_i^α) within each bulk fluid phase (aqueous: $\alpha = a$; organic: $\alpha = n$):

$$\phi \frac{\partial}{\partial t}\left(s_\alpha C_i^\alpha\right) + \phi \nabla \cdot s_\alpha \left(C_i^\alpha V^\alpha - D_\alpha^i \cdot \nabla C_i^\alpha\right) = \sum_\beta E_i^{\alpha\beta}, \quad (1)$$

where ϕ is the matrix porosity, s_α is the α-phase saturation, $D_\alpha{}^i$ is the three-dimensional hydrodynamic dispersion tensor for component i in phase α [*Bear*, 1972], V^α is the α-phase pore velocity computed using a modified form of Darcy's law [*Abriola*, 1989], and $E_i^{\alpha\beta}$ is the interphase mass exchange of component i from the β- to the α-phase. In this work, interphase mass exchange is assumed to occur only between the aqueous and organic phases (i.e., sorption to soil particles is neglected) and is approximated using a linear driving force expression [*Weber and DiGiano*, 1996]:

$$E_i^{\alpha\beta} = \kappa_l \left(C_i^{\alpha eq} - C_i^\alpha\right), \quad (2)$$

where $C_i^{\alpha\, eq}$ is the equilibrium solubility of component i in the α-phase, and κ_l is a lumped mass transfer coefficient, which quantifies the rate of mass transfer of component i from the β- to the α-phase. This lumped coefficient (κ_l) can be obtained by employing a Sherwood number ($Sh = \kappa_l {d_{50}}^2 / {D_a}^{mi}$) correlation [e.g., *Miller et al.*, 1990; *Imhoff et al.*, 1994; *Powers et al.*, 1992, 1994a] where d_{50} is the mean grain diameter, and ${D_a}^{mi}$ is the aqueous phase molecular diffusion coefficient of component i. Dissolution requires use of the specific interfacial area to account for the transient nature of mass transfer resulting from reductions in interfacial area. The specific interfacial area (a_s) of the organic phase globule was approximated with a uniform distribution of spherical globules, such that $a_s = 3/b$, where b is the NAPL globule radius. Simulations of the column experiments reported here, however, assume a pseudo-steady flow with negligible changes to NAPL volume or specific interfacial area resulting from absorption and dissolution.

[16] Writing equation (1) for the aqueous and organic phase results in two transport equations for each component i, one describing transport in the aqueous phase and one describing transport in the organic phase:

$$\phi \frac{\partial}{\partial t}\left(s_a C_i^a\right) + \phi \nabla \cdot s_a \left(C_i^a V^a - D_a^i \cdot \nabla C_i^a\right) = E_i^{an} \tag{3a}$$

$$\phi \frac{\partial}{\partial t}\left(s_n C_i^n\right) = E_i^{an}\,. \tag{3b}$$

[17] Recognizing that mass balance constraints require $E_i^{an} = -E_i^{an}$, equations (3a) and (3b) can be combined to form a single equation for component i across both the aqueous and organic phases:

$$\phi \frac{\partial}{\partial t}\left(s_a C_i^a\right) + \phi \nabla \cdot s_a \left(C_i^a V^a - D_a^i \cdot \nabla C_i^a\right) = -\phi \frac{\partial}{\partial t}\left(s_n C_i^n\right). \tag{4}$$

[18] Assuming pseudo-steady state conditions and spatially uniform saturation in one-dimensional (1-D) flow, equation (4) simplifies to the 1-D advection-dispersion equation (ADE) commonly employed in the sorption literature:

$$\frac{\partial C_i^a}{\partial t} + V^a \frac{\partial C_i^a}{\partial z} - D_a^i \frac{\partial^2 C_i^a}{\partial z^2} = -\frac{1}{m}\frac{\partial C_i^n}{\partial t}\,, \tag{5}$$

where, for NAPL partitioning, $m = \frac{s_a}{1-s_a}$ and all other parameters are as given previously.

[19] Equation (5) has been solved for a variety of interphase mass exchange conditions. Among the simplest and most commonly employed is the local equilibrium condition where concentrations of component i in the aqueous and organic phases are related algebraically using an equilibrium partitioning coefficient defined in terms of concentration $\left(K_p^{C_i}\right)$:

$$C_i^n = K_p^{C_i} C_i^a\,. \tag{6}$$

[20] Employing equation (6), equation (5) simplifies to an ADE assuming equilibrium partitioning (ADEQ):

$$R \frac{\partial C_i^a}{\partial t} + V^a \frac{\partial C_i^a}{\partial z} - D_a^i \frac{\partial^2 C_i^a}{\partial z^2} = 0\,, \tag{7}$$

where R represents the retardation factor of the contaminant, assuming equilibrium exchange with the immobile organic phase: $R = 1 + {K_p^{C_i}}/{m}$. Equation (7) is commonly employed in the sorption and PITT literature and has been solved for a variety of initial and boundary conditions [e.g., *van Genuchten and Alves*, 1982].

[21] Under conditions of kinetic interphase mass exchange, equations (2) and (3) are combined and simplified by assuming exchange is proportional to the concentration gradient between the contaminant concentration at the organic phase surface $C_i^{a^{eq}} = {C_i^n}/{K_p^{C_i}}$ and in the bulk aqueous phase (C_i^a):

$$\frac{\partial C_i^a}{\partial t} + V^a \frac{\partial C_i^a}{\partial z} - D_a^i \frac{\partial^2 C_i^a}{\partial z^2} = -\kappa_l \left(\frac{C_i^n}{K_p^{C_i}} - C_i^a\right) \tag{8a}$$

$$\frac{\partial C_i^n}{\partial t} = \kappa_l \left(\frac{C_i^n}{K_p^{C_i}} - C_i^a\right). \tag{8b}$$

[22] Equation (8), abbreviated here as the ADEK (ADE with kinetic partitioning), has again been simplified to 1-D pseudo-steady state flow and makes use of the equilibrium relation provided in equation (6) to quantify the equilibrium contaminant concentration in the organic phase. When coupled with appropriately applied initial and boundary conditions, equation (8) can be solved analytically or numerically. Models based on equation (8) are commonly referred to in the sorption literature as one-site kinetic adsorption models [e.g., *van Genuchten and Wagenet*, 1989; *Leij et al.*, 1993; *Toride et al.*, 1993]. A popular modeling program, CXTFIT, employs this model for quantifying sorption parameters [*Toride et al.*, 1999]. Note that equation (8), however, assumes that the organic phase is well mixed, and therefore does not consider the potential effect of concentration gradients present within the NAPL globule. While appropriate for certain situations, this may not always be the case, resulting in the need to model the diffusion of contaminant in the immobile organic phase.

[23] *Rasmuson and Neretnieks* [1980] used the work of *Pellett* [1964] to derive an often-employed analytical solution to equation (5) when diffusion within the immobile phase is important. In their solution, equation (5), which is derived assuming volume-averaged concentrations (C_i^a and C_i^n), is coupled to a radial diffusion equation written for the contaminant concentration ($C_i^{n^*}$) within the organic phase using the interphase mass exchange term as a boundary condition (equation (9b)) applied at the surface of the immobile organic phase ($r = b$):

$$\frac{\partial C_i^a}{\partial t} + V^a \frac{\partial C_i^a}{\partial z} - D_a^i \frac{\partial^2 C_i^a}{\partial z^2} = -\frac{1}{m}\frac{\partial C_i^n}{\partial t} \tag{9a}$$

$$\frac{\partial C_i^n}{\partial t} = -\kappa_l \left(\frac{C_i^{n*}\big|_{r=b}}{K_p^{C_i}} - C_i^a\right) \tag{9b}$$

$$\frac{\partial C_i^{n*}}{\partial t} = D_n^{mi}\left(\frac{\partial^2 C_i^{n*}}{\partial r^2} + \frac{2}{r}\frac{\partial C_i^{n*}}{\partial r}\right). \tag{9c}$$

[24] D_n^{mi} in equation (9) is the organic phase molecular diffusion coefficient of component i, r is the radial dimension, and b is the NAPL globule radius. Equation (9), abbreviated here as ADEKD (ADEK with diffusion), models the transport of contaminant in the aqueous phase undergoing partitioning to the immobile organic phase, where interphase mass exchange is controlled by both (1) resistance in the aqueous phase boundary layer separating the aqueous and organic phase (equation (9b)) and (2) resistance to mass exchange because of diffusion within the immobile organic phase (equation(9c)). Although originally derived to model adsorption because of partitioning into immobile regions of soil grains [e.g., *Rasmuson and Neretnieks*, 1981; *van Genuchten*, 1985; *Crittenden et al.*, 1986], the equations are extended in this work to model partitioning into an immobile organic phase. Table 1 summarizes the parameters employed in the diffusion model and compares the nomenclature between the sorption literature and the liquid-liquid partitioning application of this work.

[25] The described models were employed here to simulate *cis*-DCE breakthrough curves from columns contaminated with residual PCE-DNAPL. The *Brenner* [1962] solution to equation (7) published by *van Genuchten and Alves* [1982] for a finite-length column was fit to tracer tests conducted before and after the establishment of the PCE-NAPL entrapped saturation. Pre-NAPL tracer results were employed to obtain best-fit soil column porosities (ϕ), while post-NAPL tracer results were fit to determine the longitudinal dispersivity (α_L) and NAPL saturation (S_n) in each column. Gravimetrically determined values for porosity and NAPL saturation were not explicitly used; rather the experimental values guided the model fits, which were assumed to provide a better approximation of the actual column conditions. The exception here was Column A, where gravimetrically determined PCE-NAPL saturation was employed because tracer fitting produced an unreasonably high saturation ($> 20\%$). Table 2 summarizes the column parameters for all three columns employed here. All parameters other than ϕ, α_L, and S_n were independently determined through measurement or constitutive relationships available in the literature. Note that the NAPL globule radius ($b = d_{\text{eff,blob}}/2$) employed here is based on a newly formed correlation using a comprehensive survey of the literature, as described in section 3.2.

[26] Following parameter estimation from the tracer results, a solution to a nondimensionalized form of equation (9) published by *Rasmuson and Neretnieks* [1980] was employed to predict *cis*-DCE breakthrough. The Rasmuson and Neretnieks solution is described here since this use is the first application for estimating contaminant transport in a NAPL-contaminated region. Rasmuson and Neretnieks employed Laplace transforms to solve equation (9) subject to the following initial and boundary conditions:

$$C_i^a(z=0,t) = C_0 \tag{10a}$$

$$C_i^a(z=\infty,t) = 0 \tag{10b}$$

$$C_i^a(z,t=0) = 0 \tag{10c}$$

$$C_i^{n*}(r=0,z,t) \neq \infty \tag{10d}$$

$$C_i^{n*}(r,z,t=0) = 0\,. \tag{10e}$$

[27] The solution, written in nondimensional form, is:

$$\frac{C_i^a}{C_0} = \frac{1}{2} + \frac{2}{\pi}\int_0^\infty \left[\exp\left(\frac{Pe}{2} - \sqrt{\frac{\sqrt{(z^2x')^2 + (z^2y')^2} + z^2x'}{2}}\right) \times \sin\left(y\lambda^2 - \sqrt{\frac{\sqrt{(z^2x')^2 + (z^2y')^2} - z^2x'}{2}}\right)\right]\frac{d\lambda}{\lambda}\,, \tag{11}$$

with model parameters described in Table 3. Equation (11) provides an efficient, analytical solution that can be applied to solute partitioning in NAPL source zones.

[28] Equation (11) was implemented in Matlab version R2010a. Numerical integration of the infinite integral followed the methods of *Rasmuson and Neretnieks* [1981] in which the infinite integral is replaced by a finite integral with $\lambda_{\max}$ chosen as a sufficiently large upper bound. Proper model implementation was verified by comparison with other analytical [*van Genuchten and Alves*, 1982] and numerical solutions [*Toride et al.*, 1999]. It is worth noting that equation (11) can be made to approximate solutions to the simpler partitioning formulations (equations (7) and (8)). To approximate equilibrium sorption using equation (11), κ_l and D_n^{mi} are assumed to be large ($\kappa_l >> 10^{-1}$ s^{-1} and $D_n^{mi} >> 10^{-4}$ cm^2/s), such that partitioning across the aqueous phase boundary layer is nearly instantaneous and diffusion within the NAPL is rapid. If rate limited mass

Table 1. Parameter Equivalence Between Solid-Liquid Sorption Model and Liquid-Liquid Partitioning Model

Parameter	Sorption Literature Definition	Parameter	Liquid-Liquid Partitioning Definition
b (L)	Soil particle radius	b (L)	NAPL globule radius
Ds (L^2/T)	Intra-aggregate diffusivity	D_n^{mi} (L^2/T)	Diffusivity in NAPL globule
K ($L^3\,L^{-3}$)	Volume equilibrium constant	K_p^i ($L^3\,L^{-3}$)	Equilibrium partitioning coefficient
k_f (L/T)	Mass transfer coefficient	$\kappa_l a_s^{-1}$ (L/T)	Mass transfer coefficient
m (-)	$\varepsilon/(1-\varepsilon)$	m (-)	s_α/s_n
$\hat{q}$ (M/L^3)	Vol. avg. contaminant concentration in particles	C_i^n (M/L^3)	Vol. avg. contaminant concentration in NAPL globule
q_i (M/L^3)	Internal contaminant concentration in particles	$C_i^{n^*}$ (M/L^3)	Internal contaminant concentration in NAPL globule
q_s (M/L^3)	Internal contaminant concentration at particle surface ($q_i(b,z,t)$)	$C_i^{n*}\big\vert_{r=b}$ (M/L^3)	Internal contaminant concentration at NAPL surface ($C_i^{n^*}(b,z,t)$)
r (L)	Radial distance from center of spherical soil particle	r (L)	Radial distance from center of spherical NAPL globule
ε ($L^3\,L^{-3}$)	Soil porosity	n ($L^3\,L^{-3}$)	Soil porosity

Table 2. Column Parameters

	Column		
	A	B	C
Sand size (ASTM sieve sizes)	50–60	45–50	20–30
Range of grain diameter (μm)	250–300	300–355	600–850
Median grain size diameter (d_{50}) (μm)	275	328	725
Uniformity index (U_i)	1.10	1.09	1.20
Column diameter (d_c) (cm)	4.80	4.80	4.80
Column length (L) (cm)	3.50	3.45	3.50
Porosity (n) (L_{void}/L_{total})	0.388	0.377	0.360
Pore volume (PV) (mL)	24.6	23.5	22.8
PCE-NAPL saturation (S_n) (%)	17.1	13.2	11.1
PCE-NAPL volume (V_n) (mL)	4.20	3.10	2.53
PCE-NAPL ganglia radius (b)[a] (μm)	128	141	263
Volumetric flow rate (Q) (mL/min)	2.00	2.00	2.00
Darcy velocity (q) (cm/sec)	1.84×10^{-3}	1.84×10^{-3}	1.84×10^{-3}
Pore water velocity (v) (cm/s)	5.72×10^{-3}	5.63×10^{-3}	5.75×10^{-3}
Longitudinal dispersivity (α_L) (cm)	1.76×10^{-1}	8.13×10^{-2}	3.37×10^{-1}
Diffusivity of *cis*-DCE in the aqueous phase (D_a)[b] (cm^2/sec)	1.07×10^{-5}	1.07×10^{-5}	1.07×10^{-5}
Diffusivity of *cis*-DCE in PCE-NAPL (D_n)[b] (cm^2/sec)	1.21×10^{-5}	1.21×10^{-5}	1.21×10^{-5}
cis-DCE partition coefficient (K_p) (L_{aq}/L_{NAPL})	105	105	105
Retardation factor (equilibrium partitioning) (R_c) (-)	22.6	16.9	14.1
Modified Sherwood number (Sh') (-)	0.246	0.305	0.856
Lumped mass transfer coefficient (k_l) (s^{-1})	3.49×10^{-3}	3.05×10^{-3}	1.75×10^{-3}
cis-DCE pulse concentration (C_0) (mg/L)	166	167	166
Pulse duration (t_0) (min)	208.90	208.60	205.34
Experiment duration (t_f) (min)	652.21	656.43	654.44
cis-DCE recovery in effluent (%)	101.3	101.0	99.2
cis-DCE mass balance[c] (%)	102.0	101.2	101.0

[a]Model assumes PCE-NAPL distributed as a uniform population of spheres having radius b as estimated using equation (12).
[b]Estimated at 22°C using the correlation of *Hayduk and Laudie* [1974].
[c]Summation of mass recovered in column effluent and that was quantified during a postexperiment extraction of the column.

transfer is expected, but diffusive limitations within the NAPL are negligible, equation (11) is simplified to the kinetic equation (equation (8)) by assuming D_n^{mi} is large. Global mass balance calculations confirmed that errors because of numerical integration were never more than 1%.

3. Results and Discussion

3.1. Liquid-Liquid Equilibrium

[29] The ternary phase data for water, *cis*-DCE, and PCE at 22 ± 0.1 °C depicted in Figure 1 were employed to establish the thermodynamic driving force for the partitioning of *cis*-DCE between DNAPL and the aqueous phase. The interested reader is referred to the work of *Sørensen et al.* [1979] for a summary of ternary phase diagrams within the context of liquid-liquid equilibria. In addition, the work of *Ramsburg and Pennell* [2002], and the references contained therein, summarize the environmental relevance of liquid-liquid equilibria. The data shown in Figure 1 demonstrate that this study explores the range of possible compositions, and that most mixtures of *cis*-DCE, PCE, and water produce two phases, one organic phase and one aqueous phase, which can be predicted using UNIFAC (dashed lines). The dominance of the two-phase region is not surprising given the low solubilities of PCE and *cis*-DCE in water (measured mole fractions of $(2.39 \pm 0.07) \times 10^{-5}$ and $(9.77 \pm 0.24) \times 10^{-4}$, respectively) and low solubility of water in PCE and *cis*-DCE (measured mole fractions of $(6.28 \pm 0.17) \times 10^{-4}$ and $(4.55 \pm 0.14) \times 10^{-3}$, respectively). It is noted, however, that there are also two, single-phase regions

Table 3. Nomenclature Employed in ADEKD Solution (Equation (11))

Input	Intermediate Parameters		
λ	$H_{D1}(\lambda) = \lambda\left(\frac{\sinh(2\lambda)+\sin(2\lambda)}{\cosh(2\lambda)+\cos(2\lambda)}\right) - 1$		$H_1(\lambda,\nu) = \frac{H_{D1} + \nu\left(H_{D1}^2 + H_{D2}^2\right)}{(1+\nu H_{D1})^2 + \left(\nu H_{D2}^2\right)}$
	$H_{D2}(\lambda) = \lambda\left(\frac{\sinh(2\lambda)+\sin(2\lambda)}{\cosh(2\lambda)+\cos(2\lambda)}\right)$		$H_2(\lambda,\nu) = \frac{H_{D2}}{(1+\nu H_{D1})^2 + \left(\nu H_{D2}^2\right)}$
$\kappa_l a_s^{-1}$ (L/T)	$R_f = b/3k_i^{an}$	$v = \gamma R_f$	
b (L) D_n^{mi} (L^2/T) K_p^{Ci} $(L^3\,L^{-3})$	$\sigma = 2D_n^{mi}/b^2$	$y = \sigma t$	$z^2x' = Pe\left(Pe/4 + \delta H_1\right)$
	$\gamma = 3D_n^{mi}K_p^i/b^2$	$\delta = \gamma z/mV$	$z^2y' = \delta Pe\left(2\lambda^2/3R' + H_2\right)$
m (-)	$R' = K_p^{C_i}/m$		
V (L/T) $D^i{}_a(L^2/T)$ z (L)	$Pe = zV/D_a^i$		

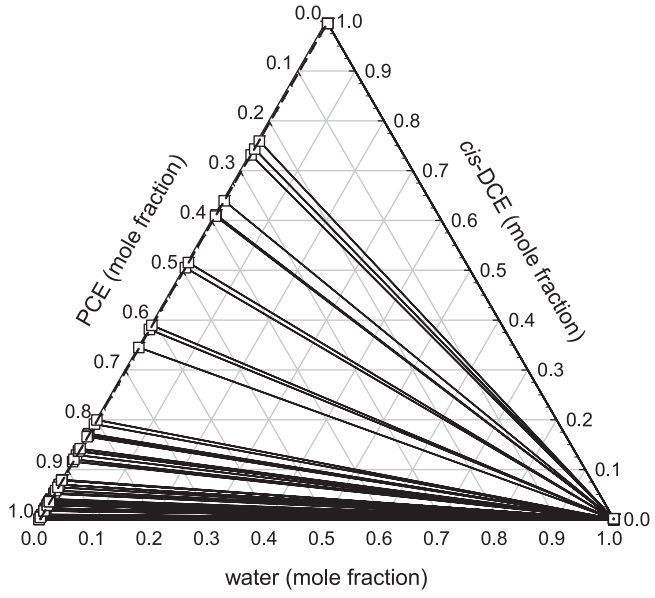

Figure 1. Phase diagram for the water/*cis*-DCE/PCE ternary at 22 ± 0.1°C with measured tie-lines (solid lines connecting squares), and UNIFAC prediction of binodal curves (dashed line).

within this type II system comprising two partially miscible pairs (water−PCE and water−*cis*-DCE) and one miscible pair (*cis*-DCE−PCE). These two single-phase regions fall along the PCE and *cis*-DCE axes, though the binodal curves defining these regions terminate on the water axis. The NAPL and aqueous binodal curves extend from $((6.28 \pm 0.17) \times 10^{-4}, 0, (9.995 \pm 0.001) \times 10^{-1})$ to $((4.55 \pm 0.14) \times 10^{-3}, (9.956 \pm 0.001) \times 10^{-1}, 0)$ and $((9.9997 \pm 0.0001) \times 10^{-1}, 0, (2.39 \pm 0.07) \times 10^{-5})$ to $((9.990 \pm 0.001) \times 10^{-1}, (9.77 \pm 0.24) \times 10^{-4}, 0)$, respectively, where ternary triplets are defined as $(x_{\text{water}}, x_{cis\text{-DCE}}, x_{\text{PCE}})$.

[30] The distribution of *cis*-DCE between a PCE-DNAPL and aqueous phase holds more relevance when considering product partitioning during reductive dechlorination processes [*Ramsburg et al.*, 2010]. Examination of the partitioning of *cis*-DCE between the DNAPL and aqueous phases over all possible mole fractions (Figure 2) suggests that the partition coefficient, as defined on a mole fraction basis, $K_p^{x_i}$, is a function of composition. The compositional dependence of the partition coefficient is bound by two linear models: one established by *Ramsburg et al.* [2010] and another that is described by the Raoult's Law analogy (Figure 2). These models capture the behavior at either extreme and represent the assumptions of ideal dilute solution (Henry's Law) and ideal solution (Raoult's Law analog). Thus, the $K_p^{x_i}$ reported at low mole fractions $(K_p^{x_i} = 593 \pm 5 \frac{mol_{\text{total}}^{\text{aq}}}{mol_{\text{total}}^{\text{NAPL}}})$ represents a Henry's Law coefficient for the liquid-liquid partitioning (Figure 2) [*Ramsburg et al.*, 2010]. The partition coefficient produced using the Raoult's Law analogy $(K_p^{x_i,RLA} = 1006 \pm 25 \frac{mol_{\text{total}}^{\text{aq}}}{mol_{\text{total}}^{\text{NAPL}}})$ employs the measured, aqueous solubility of *cis*-DCE $(x_{\text{cis-DCE}}^{\text{aq}} = (0.977 \pm 0.24) \times 10^{-3})$, and is therefore higher than that previously reported [*Ramsburg* et al., 2010]. The observation of a rather limited transition region $(0.15 \times 10^{-3} < x_{\text{cis-DCE}}^{\text{aq}} < 0.40 \times 10^{-3})$ suggests that these two limiting assumptions can describe much of the real solution behavior that results from a balance between chemical (e.g., hydrogen bonding) and physical (e.g., electrostatic, induction, dispersion) interactions occurring between the components of the phases. Below $x_{\text{cis-DCE}}^{\text{aq}} = 0.15 \times 10^{-3}$, hydrogen bonding between *cis*-DCE and water within the aqueous solution enhances the solubility of *cis*-DCE in the aqueous phase (negative deviation from ideal solution behavior, lower $K_p^{x_i}$). In this range of aqueous mole fractions, the aqueous phase can be assumed to be dilute. Using the phase densities (ρ_{aq} and ρ_{NAPL}) and average molecular weights of the phases (MW_{aq} and MW_{NAPL}) to convert $K_p^{x_i}$ to a concentration basis partition coefficient $\left(K_p^{C_i} = K_p^{x_i} \frac{\rho_{NAPL}}{\rho_{aq}} \frac{MW_{aq}}{MW_{NAPL}}\right)$ produces $K_p^{C_i} = 105 \frac{L_{aq}}{L_{NAPL}}$ (Table 2). Above $x_{cis\text{-}DCE}^{aq} = 0.40 \times 10^{-3}$, this hydrogen bonding is counterbalanced by the electrostatic, induction, and dispersion forces present within the aqueous phase and NAPL (positive deviations balance negative deviations, making the ideal solution model a good approximation). UNIFAC is unable to capture this transition and balance (Figure 2), but does provide a reasonable estimate for $K_p^{x_i}$ at low concentrations (Figure 2) [*Ramsburg et al.*, 2010].

3.2. Column Experiments

[31] A series of three column studies was conducted to elucidate the kinetics of *cis*-DCE mass exchange during aqueous-phase flow. Visualization studies of NAPL ganglia entrapped within natural porous media indicate NAPL ganglia size and shape depend upon characteristics of the porous medium (e.g., d_{50}, U_i, θ_{NAPL}) [*Conrad et al.*, 1992; *Powers et al.*, 1992; *Schnaar and Brusseau*, 2005; *Brusseau et al.*, 2009]. The fact that uniform medium to fine grain sands produce populations characterized by a large fraction of singlets was the basis for the selection of the porous media employed herein [*Schnaar and Brusseau*, 2005]. That is, we employ three, relatively uniform, size fractions of Ottawa sand to control the effective diameter of entrapped DNAPL ganglia (and therefore diffusion length within the DNAPL). The median grain size diameter (d_{50}) of the media employed in the column experiments increase from Column A to Column C (Table 2). Recently, *Brusseau et al.* [2009] correlated effective blob or ganglia diameter to particle diameter. This correlation holds promise because it uses median grain size as a marker for pore size, which physically constrains blob size. The *Brusseau et al.* [2009] correlation, however, does not consider other factors such as uniformity index or maximum entrapped saturation, both of which have been observed to influence the size, shape, and distribution of NAPL ganglia [*Powers*, 1992]. Moreover, when the method of *Brusseau et al.* [2009] is expanded to consider existing data for the effective size of NAPL ganglia entrapped within natural porous media [*Powers*, 1992; *Schnaar and Brusseau*, 2005; *Brusseau et al.*, 2009] the linear correlation to median grain size begins to break down ($R^2 = 0.909$, data not shown), particularly for the coarser media examined by *Powers* [1992].

[32] Median grain size (d_{50}), particle uniformity index (U_i), and volumetric content of entrapped NAPL (θ_{NAPL})

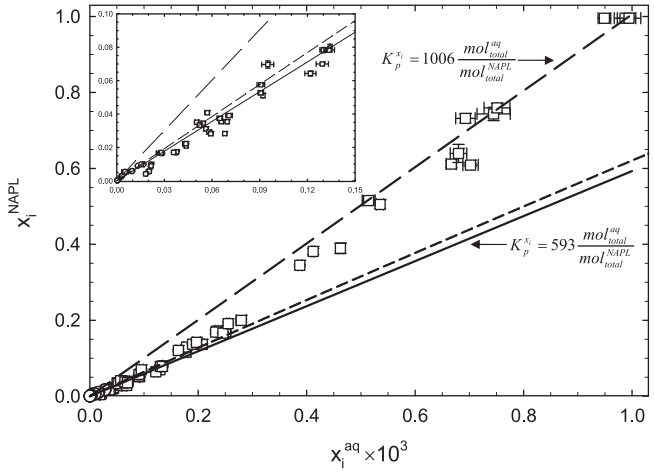

Figure 2. Distribution of *cis*-DCE between DNAPL and the aqueous phase at 22 ± 0.1 °C. Data spanning all possible mole fractions of *cis*-DCE include this study (squares) and *Ramsburg et al*. [2010] (circles). Error bars represent the standard error of triplicate measurements. Models include ideal dilute solution [*Ramsburg et al*., 2010] (solid line), ideal solution (long dashed line), and UNIFAC simulation (short dashed line). Inset shows the dilute range represented by $x_i^{aq} < 1.5 \times 10^{-4}$ and $x_i^{NAPL} < 0.1$.

are often employed in mass transfer correlations as a surrogate for interfacial area. Given the relationship between interfacial area and blob size and configuration, these same parameters (d_{50}, U_i, and θ_{NAPL}) were employed to develop a new correlation for effective blob size. Results of a nonlinear least squares correlation ($R^2 = 0.964$) process are shown in Figure 3 for existing data on the effective size of NAPL ganglia entrapped within natural porous media [*Powers*, 1992; *Schnaar and Brusseau*, 2005; *Brusseau et al.*, 2009]. The new correlation produced through the regression is shown as equation (12):

$$d_{\text{eff,blob}} = 3.59 \cdot (d_{50})^{0.86} (U_i)^{-0.17} (\theta_{NAPL})^{0.20} . \qquad (12)$$

[33] The strong dependence of the correlation on median grain size is consistent with the concept that the structure of the porous medium controls NAPL blob size [*Brusseau et al.*, 2009]. The correlation, however, also highlights that all else being equal, effective blob size increases with increasing entrapped NAPL saturation. Smaller pores are more effective at entrapping NAPL (because of higher capillary forces) so correlation against median grain size and entrapped NAPL saturation breaks down for graded materials. The correlation represented by equation (12) is consistent with the idea that effective blob size should decrease with increasing uniformity index because of the variation of pore sizes that is inherent in media characterized by larger uniformity indices. The effective blob diameters calculated using equation (12) increase from Column A to Column C (Table 2).

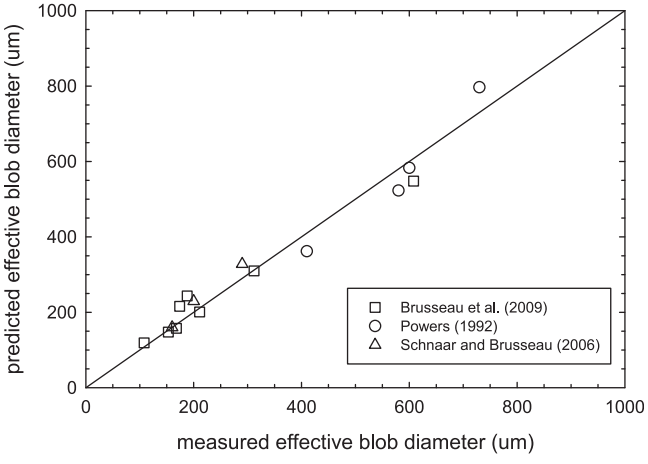

Figure 3. Measured versus predicted blob diameters using the correlation shown in equation (12).

[34] Mass transfer rate limitations within the aqueous phase are characterized here using correlations based upon pure component dissolution [*Powers et al.*, 1992; *Imhoff et al.*, 1994]. An important aspect of this work is the assessment of these correlations for use in absorption and dissolution of solutes present in both the aqueous phase and DNAPL. The governing equations employed herein also incorporate a diffusional resistance to mass exchange within the DNAPL. When compared to the ADEK, the additional resistance presented by intra-NAPL diffusion is expected to result in shorter *cis*-DCE mean column residence times (because of the increased resistance to mass transfer, resulting in a smaller fraction of the *cis*-DCE partitioning into the NAPL) and greater tailing (because of the longer NAPL residence times for the fraction of the *cis*-DCE mass that does partition into the NAPL). Parameters for each of the three column experiments are provided in Table 2.

[35] Breakthrough curves (BTCs) obtained from Column A (Figure 4) and Column B (Figure 5) are similar (center of mass at 23.4 and 23.5 pore volumes, respectively, and skewness of 0.333 and 0.421, respectively), but the BTC from Column C (Figure 6) suggests less partitioning (center of mass at 20.9 pore volumes) and greater tailing (skewness of 1.72). Also shown in Figures 4–6 are predictions of the *cis*-DCE BTCs assuming nonreactive transport (equation (7), $R = 1$), equilibrium partitioning (equation (7)), and

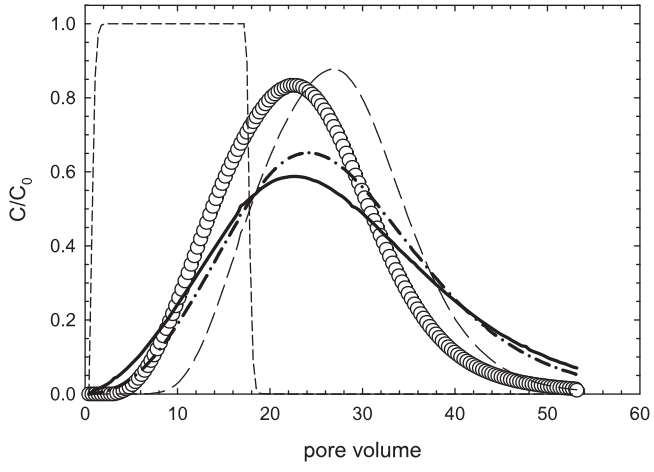

Figure 4. Normalized effluent concentrations of *cis*-DCE and model predictions for Column A: data (circles), nonreactive pulse (short dashes), local equilibrium assumption (long dashes, 0.161), rate limited with *Powers et al.* [1992] correlation (solid line, 0.129) and rate limited with *Imhoff et al.* [1994] correlation (dashes and dots, 0.120). Numerical values represent the root mean square differences between the data and each simulation of *cis*-DCE partitioning.

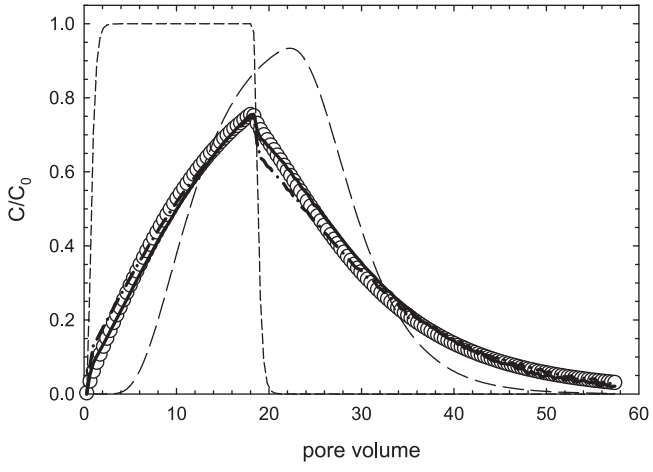

Figure 6. Normalized effluent concentrations of *cis*-DCE and model predictions for Column C: data (circles), nonreactive pulse (short dashes), local equilibrium assumption (long dashes, 0.162), rate limited with *Powers et al.* [1992] correlation (solid line, 0.017) and rate limited with *Imhoff et al.* [1994] correlation (dashes and dots, 0.023). Numerical values represent the root mean square differences between the data and each simulation of *cis*-DCE partitioning.

rate-limited mass transfer (equation (11)). The nonreactive transport simulation is provided to illustrate the pulse duration and dispersivity. Equilibrium simulations suggest that all of the observed BTCs result from kinetic exchange (retardation factors resulting from the partitioning are reported in Table 2).

[36] Kinetic exchange of *cis*-DCE mass between the aqueous phase and PCE-DNAPL was modeled using a mass transfer coefficient for the aqueous phase resistance and diffusion within spherical PCE-DNAPL ganglia for resistance within the NAPL. Use of a mass transfer coefficient presumes knowledge of an appropriate Sherwood number correlation. While there has been significant research related to pure component dissolution from entrapped ganglia assuming constant and time variant DNAPL saturations [e.g., *Miller et al.*, 1990; *Powers et al.*, 1992; *Geller and Hunt*, 1993; *Powers et al.*, 1994a; *Imhoff et al.*, 1994], little consideration has been given to whether or not these correlations hold for conditions of absorption and subsequent dissolution [*Brusseau*, 1992; *Hatfield and Stauffer*, 1993]. Here we employ two of these correlations, from the work of *Powers et al.* [1992] and *Imhoff et al.* [1994], under conditions where the PCE-DNAPL saturation is presumed to be entrapped and constant through time. The *Powers et al.* [1992] and *Imhoff et al.* [1994] correlations were selected because these correlations were developed from column experiments in which PCE- and TCE-DNAPL saturations, respectively, were entrapped using an imbibition and drainage procedure similar to that employed here. The dissolution length present in the *Imhoff et al.* [1994] correlation is interpreted here as the zone within the column over which mass transfer is occurring. In contrast to dissolution, where this dissolution length is bounded by regions of the column containing (near) zero and initial saturations, absorption and dissolution of *cis*-DCE by/from the PCE-DNAPL were assumed to occur over the entire column length (i.e., $x = L$). Interestingly, neither correlation is strictly valid for our experimental conditions (Table 4). Thus, use of either correlation (Figures 4–6) represents an extrapolation in phenomenology (i.e., kinetics for absorption and dissolution are similar) and utility (i.e., models can be extended outside of the range of parameters employed for their development). That notwithstanding, the greater applicability of the *Powers et al.* [1992] model for Column C (given the values of Re (or Re') and d_{50}) provides a remarkable prediction of the breakthrough curve (Figure 6).

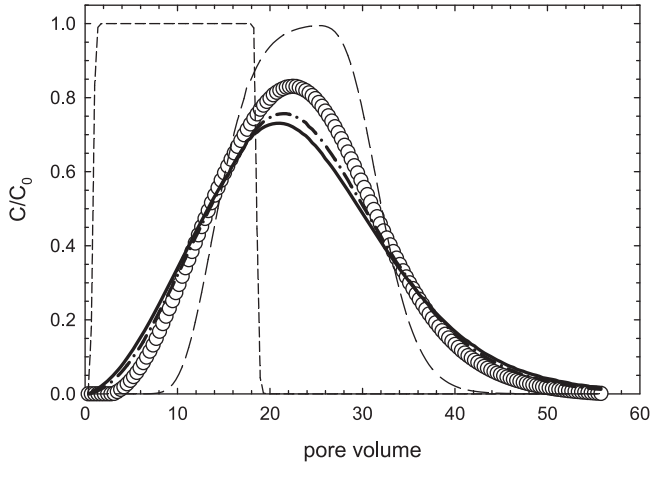

Figure 5. Normalized effluent concentrations of *cis*-DCE and model predictions for Column B: data (circles), nonreactive pulse (short dashes), local equilibrium assumption (long dashes, 0.129), rate limited with *Powers et al.* [1992] correlation (solid line, 0.060) and rate limited with *Imhoff et al.* [1994] correlation (dashes and dots, 0.043). Numerical values represent the root mean square differences between the data and each simulation of *cis*-DCE partitioning.

Table 4. Comparison of Experimental Parameters to Those Employed for Mass Transfer Correlations

	Re (-)	*Re′* (-)	θ_{NAPL} (L_{NAPL}/L_{total})	U_i (-)	x/d_{50} (-)	d_{50} (μm)
Powers et al. [1992]	0.012–0.200	0.045–0.593	0.032–0.064	1.19–3.46	-	450–1200
Imhoff et al. [1994]	0.00044–0.00654	0.001–0.021	< 0.040	1.19	1.40–180	360
Column A	0.0053	0.0164	0.066	1.10	48.2	275
Column B	0.0062	0.0190	0.045	1.09	127	328
Column C	0.0140	0.0436	0.040	1.20	105	725

[37] While predictions for Columns A and B do not match the data as closely as those for Column C, use of the *Imhoff et al.* [1994] correlation results in better description of the *cis*-DCE transport observed in Columns A and B (given the values of *Re* (or *Re′*) and d_{50}) (Figures 4–6, note that the root mean square differences between the data and each simulation are provided in the captions). The poorer performance of the model and overprediction of partitioning for Column A was unexpected, given that this column was constructed using a medium that should entrap PCE-DNAPL as relatively small, singlet blobs [*Brusseau et al.*, 2009]. That is, it was thought that conditions in Column A best matched the key assumptions present in the model. Given the similarities between the BTCs and porous media for Columns A and B, the difference in PCE-DNAPL saturations (17.1% and 13.2%, respectively) opens questions related to the errors in the saturation measurement and accessibility of the DNAPL. Additional simulations were conducted to explore each of these possibilities. Use of the saturation obtained in Column B to predict the transport observed in Column A better captures the center of mass and peak height of experimental data, but does little to adjust the shape as assessed through the standard deviation of the simulated BTC ($\sigma_{sn=0.171} = 9.7$ and $\sigma_{sn=0.132} = 9.6$) (Figure 7). Thus, an accessibility parameter (f) was added to modify the interfacial area (a_s) as described in *Powers et al.* [1994b] and used as an adjustable parameter to fit the model to the effluent data from Columns A and B. Fits suggest 34% and 67% of the interfacial area was accessible for mass transfer in Columns A and B, respectively (Figures 7 and 8). These fitting results are consistent with observations and simulations provided in the NAPL dissolution studies of *Johns and Gladden* [1999] and *Powers et al.* [1994b] that report percentages of accessible interfacial area ranging from 30% to 72% and from 48% to 94%, respectively. Intriguingly, the finest sand fraction (Column A) appears to result in the least accessible PCE-DNAPL, that is, DNAPL that was thought to be distributed primarily as singlets [*Brusseau et al.*, 2009], and the coarsest fraction (Column C) appears to result in the most accessible PCE-DNAPL, that is, DNAPL that was thought to comprise a distribution of singlet and multipore ganglia [*Powers*, 1992].

[38] We hypothesize that the accessibility of DNAPL in all columns is limited (i.e., not all DNAPL is available for mass exchange). This hypothesis suggests that the capability of the model to predict the BTC observed in Column C (a medium where ganglia exist as singlets and multipore shapes) results from competing effects that allow the simple assumption of a uniform population of spherical DNAPL blobs to accurately describe the accessible interfacial area. Ganglia distributed across multiple pores have less specific interfacial area relative to that of an equivalent DNAPL volume, but a greater number of entrapped singlets. Shape factors have been employed to gauge the amount that ganglia deviate from a spherical shape, with spheres representing an upper bound at a shape factor equal to 1 [*Mayer and Miller*, 1992]. In short, values less than unity suggest that the fluid-specific interfacial area (i.e., surface area per volume of entrapped fluid) for any one blob is larger than that

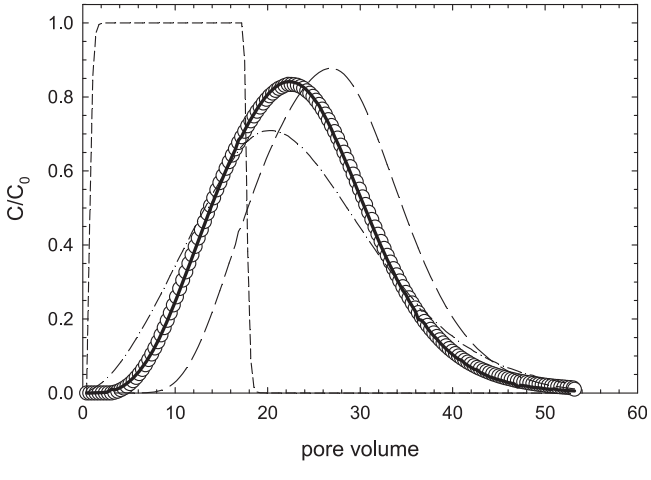

Figure 7. Model fits for Column A: data (circles), nonreactive pulse (short dashes), local equilibrium assumption (long dashes), rate limited with an S_n of 13.2% and 100% accessibility (dashes and dots), rate limited with an S_n of 13.2% and 34% accessibility (solid line).

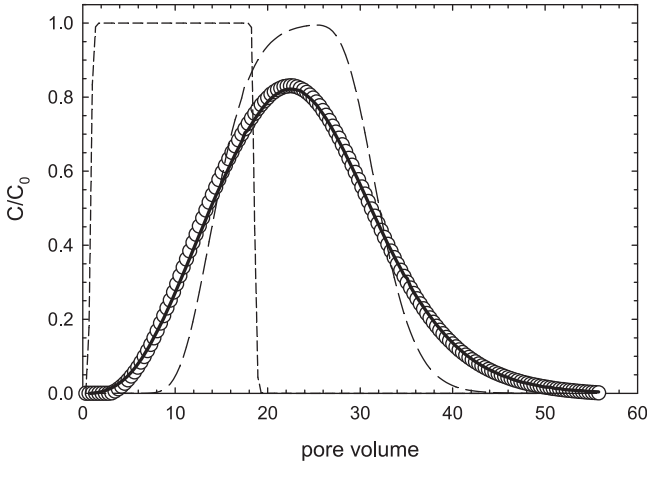

Figure 8. Model fit for Column B: data (circles), nonreactive pulse (short dashes), local equilibrium assumption (long dashes), rate limited with 67% accessibility (solid line).

represented by the effective sphere assumption (i.e., *3/b*). Consider, for example, the specific interfacial area formed by a sphere and that formed by an oblate spheroid having the same volume. The oblate spheroid has greater fluid specific interfacial area because the volume is held as a constant. Studies employing shape factors when characterizing entrapped ganglia, however, often compare the volume of a blob to the volume of the smallest sphere which can enclose the blob [*Mayer and Miller*, 1992; *al-Raoush and Willson*, 2005]. Because this comparison is based upon shapes of unequal volume, the use of the effective blob diameter underestimates the total number of oblate or complex ganglia for a given nonwetting phase saturation. Thus, use of the effective blob diameter may underestimate the total (fluid-specific) interfacial area. Studies examining the shape factors of entrapped nonwetting phase ganglia suggest: (1) shape factors decrease with increasing effective blob size [*Mayer and Miller*, 1992]; and (2) that values for large, entrapped blobs, as well as average values, can be low (0.25 and 0.32, respectively) for media of similar size as the medium employed in Column C [*Mayer and Miller*, 1992; *al-Raoush and Willson*, 2005]. These observations suggest that the actual fluid-specific interfacial area for nonspherical ganglia may be 3 to 4 times greater than that suggested by the effective sphere assumption. Thus, the effects of accessibility (i.e., limited interfacial area for solute exchange) and number (i.e., underestimation of interfacial area per volume NAPL) of ganglia may counteract one another in the coarser medium employed in Column C. The result is an accurate, though perhaps fortuitous, prediction of solute transport using the effective blob diameter, which highlights the need to continue efforts that attempt to link imaging of porous media to thermodynamic descriptions of interfacial area [*Porter et al.*, 2010]

3.3. Sensitivity Analysis

[39] The inclusion of resistance to mass transfer across the aqueous film boundary layer (film resistance) and within the immobile NAPL globule (diffusion resistance) in the *Rasmuson and Neretnieks* [1980] solution facilitates the identification of conditions under which film or diffusion mass transfer resistance control. *Crittenden et al.* [1986] employed a Biot number (*Bi*) to examine mass transfer resistance when considering intra-aggregate diffusion and *Willson et al.* [2000] applied the *Bi* concept to examine mass transfer resistance in a partitioning tracer test:

$$Bi = {}^{1}/_{m\nu} \tag{13}$$

where *Bi* (equation (13)) is defined using the nomenclature in this work (Table 3). *Crittenden et al.* [1986] suggested that when the *Bi* is high (> 20), intra-aggregate diffusion controls the overall rate of mass exchange. Conversely, when *Bi* is low (< 1), film resistance controls the kinetics of mass exchange. Applying equation (13) to describe the columns here suggests film resistance in the aqueous phase is the dominant mass transfer process (*Bi* in column A: 3.1×10^{-5}, column B: 2.4×10^{-5}, and column C: 4.0×10^{-5}). However, the combination of aqueous phase resistance and NAPL resistance to mass transfer mixes assumptions about the interface. The use of mass transfer coefficients and the linear driving force model presumes that curved interfaces can be modeled as planes. Diffusion within fluid droplets is typically modeled by solving the diffusion equation in spherical coordinates. Moreover, the Biot number criteria we have described linearize both the diffusion time scale and time scale for transport through the envisioned aqueous boundary layer (i.e., linear driving force model). Thus, these previously considered Biot number criteria fail to capture the role of curvature, particularly for small droplets, and may not accurately describe the relative importance of the exchange processes [*Alvarez et al.*, 2010].

[40] Simulations depicted in Figure 9 use the model to explore the relative contribution of diffusion across the aqueous phase boundary layer and within the NAPL globule by adjusting the magnitude of the lumped mass transfer coefficient (κ_l) and/or the diffusion coefficient of *cis*-DCE in the NAPL (D_n^{mi}). The original simulation for Column C serves as the baseline for this sensitivity analysis (see Table 2 for parameters). Increasing or decreasing the lumped mass transfer coefficient while holding all else constant appears to transition the curve between the conservative (no partitioning) simulation and the equilibrium partitioning simulation. Increasing the lumped mass transfer coefficient ($\kappa_l \times 10^2$) results in nearly equilibrium partitioning (simulation not shown). In contrast, decreasing the lumped mass transfer coefficient ($\kappa_l \times 10^{-1}$) results in a lower peak concentration and extended tailing as partitioning of *cis*-DCE from the PCE-DNAPL is slowed (Figure 9). Further decrease in the lumped mass transfer coefficient ($\kappa_l \times 10^{-2}$) results in nearly conservative breakthrough (simulation not shown). Increases to the organic phase diffusion coefficient, while holding all else constant, have no visual effect on the simulated breakthrough of *cis*-DCE (simulation not shown). Decreasing the organic phase diffusion coefficient ($D_n^{mi} \times 10^{-3}$) results in less *cis*-DCE partitioning and extended tailing (Figure 9). In fact, further decrease to the organic phase diffusion coefficient ($D_n^{mi} \times 10^{-4}$) results in a simulation that appears to be a smoothed approximation of that obtained with $\kappa_l \times 10^{-1}$ (Figure 9).

[41] Although the column simulations and *Bi* suggest the experimental conditions employed here were dominated by mass transfer resistance in the aqueous phase, the model may be used to examine conditions in which resistance in the aqueous and organic phase are important. Decreasing the lumped mass transfer coefficient ($\kappa_l \times 10^{-1}$) while simultaneously decreasing the diffusivity in the organic phase ($D_n^{mi} \times 10^{-3}$) result in a simulated *cis*-DCE BTC that deviates from that simulated, with no change to the diffusivity ($D_n^{mi} \times 10^{0}$) and the same decrease to the mass transfer coefficient ($\kappa_l \times 10^{-1}$) (Figure 9). This deviation results from greater diffusive limitation, albeit artificial, within the NAPL, and occurs at a $Bi \sim 4 \times 10^{-3}$, well below the established criterion ($Bi < 1$) that is indicative of systems where film transfer controls the overall kinetics. Similarly, simulation results for the case where the lumped mass transfer coefficient was increased ($\kappa_l \times 10^1$) and the diffusivity in the organic phase was decreased ($D_n^{mi} \times 10^{-2}$) suggest that resistances in both phases may be active (compare to $\kappa_l \times 10^1$, $D_n^{mi} \times 10^0$ curve), despite having a *Bi* of 4.0×10^{-2} (Figure 9). These results indicate that care must be taken to understand the conditions controlling mass transfer and that employing a model capable of capturing

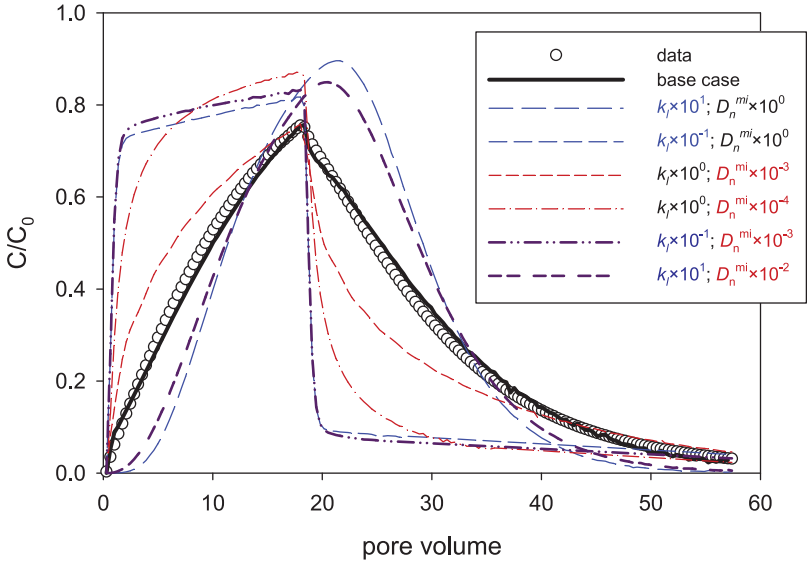

Figure 9. Model sensitivity using the conditions present in Column C as the base case.

resistance in both the aqueous and the organic phase will better facilitate accurate contaminant predictions.

4. Conclusions

[42] Results from the batch experiments indicate that chlorinated ethene NAPLs have substantial potential to sequester *cis*-DCE under equilibrium conditions, even though the partition coefficient is lower at lower concentrations. A linear simplification of the partitioning at low concentration, representing an ideal dilute solution, was found to suitably describe the partitioning when aqueous concentrations of *cis*-DCE are less than approximately 8 mM. This finding suggests that the linear simplification for the concentration-based partition coefficient describing the dilute region ($K_p^{C_i} = 105\frac{L_{aq}}{L_{NAPL}}$) may aid in predicting the distribution of *cis*-DCE at most DNAPL sites employing metabolic reductive dechlorination.

[43] Existing, dissolution-based correlations for mass transfer coefficients were found to capture the kinetics of the absorption and dissolution of *cis*-DCE when examined in column studies containing uniformly entrapped PCE-DNAPL. More study is, however, required to assess the potential influences of flow bypassing and slower mass exchange in regions of higher DNAPL saturation. Sensitivity analyses suggest diffusion within DNAPL ganglia has negligible influence on aqueous phase transport, implying that a single aqueous phase resistance, in the form of a linear driving force, can capture the transport of degradation products within ganglia dominated source zones. Validation of these frequently employed assumptions should increase confidence placed in the results obtained using multiphase compositional simulators when modeling the metabolic reductive dechlorination process occurring within DNAPL source zones. Moreover, experimental and simulation results highlight the possibility of using these simulators to develop conceptual designs for amendment delivery (type and dose of amendment to limit organism toxicity and maximize degradation within dechlorinating consortia).

[44] **Acknowledgments.** The authors gratefully acknowledge the contributions of Ms. Christine Thornton and Ms. Katherine Muller. The authors also wish to acknowledge the constructive comments provided by the anonymous reviewers. Support for this project was provided by National Science Foundation Awards EAR 0711344 and EAR 0711450. Any opinions, findings, and conclusions or recommendations expressed in this material are those of the authors and do not necessarily reflect the views of the National Science Foundation.

References

Abriola, L. M. (1989), Modeling multiphase migration of organic chemicals in groundwater systems—A review and assessment, *Environ. Health Perspec.*, *83*, 117–143.

Adamson, D. R., D. Y. Lyon, and J. B. Hughes (2004), Flux and product distribution during biological treatment of tetrachloroethene dense nonaqueous phase liquid, *Environ. Sci. Technol.*, *39*(7), 2021–2028, doi:10.1021/es034737a.

al-Raoush, R. I. and, C. S. Willson (2005), A pore-scale investigation of multiphase porous media system, *J. Contam. Hydrol.*, *77*(1–2), 67–89, doi:10.1016/j.jconhyd.2004.12.001.

Alvarez, N. J., L. M. Walker, and S. L. Anna (2010), Diffusion-limited adsorption to a spherical geometry: The impact of curvature and competitive time scales, *Phys. Rev. E*, *82*(1), 011604, doi:10.1103/PhysRevE.82.011604.

Amos, B. K., J. A. Christ, L. M. Abriola, K. D. Pennell, and F. E. Löffler (2007), Experimental evaluation and mathematical modeling of microbially enhanced tetrachloroethene (PCE) dissolution, *Environ. Sci. Technol.*, *41*(3), 963–970. doi: 10.1021/es061438n.

Amos, B. K., E. J. Suchomel, K. D. Pennell, and F. E. Löffler (2008), Microbial activity and distribution during contaminant dissolution from a NAPL source zone, *Water Res.*, *42*(12), 2963–2974, doi: 10.1016/j.watres.2008.03.015.

Annable, M. D., P. S. C. Rao, K. Hatfield, W. D. Graham, A. L. Wood, and C. G. Enfield (1998), Partitioning tracers for measuring residual NAPL: field-scale test results, *J. Environ. Eng. 124*(6), 498–503.

Bear, J. (1972), *Dynamics of Fluids in Porous Media*, Dover, New York.

Brenner, H. (1962), The diffusion model of longitudinal mixing in beds of finite length—Numerical values, *Chem. Eng. Sci.*, *17*(4), 229–243.

Brusseau, M. L. (1992), Rate-limited mass-transfer and transport of organic solutes in porous-media that contain immobile immiscible organic liquid, *Water Resour. Res.*, *28*(1), 33–45.

Brusseau, M. L., M. Narter, S. Schnaar, and J. Marble (2009), Measurement and estimation of organic-liquid/water interfacial areas for several natural porous media. *Environ. Sci. Technol.*, *43*(10), 3619–3625, doi:10.1021/es8020827.

Carr, C. S., S. Garg, and J. B. Hughes (2000), Effect of dechlorinated bacteria on the longevity and composition of PCE-containing nonaqueous

phase liquids under equilibrium dissolution conditions, *Environ. Sci. Technol.*, *34*(6), 1088–1094.

Carta, G., and J. S. Bauer (1990), Analytic solution for chromatography with nonuniform sorbent particles, *AIChE J.*, *36*(1), 147–150.

Christ, J. A. and L. M. Abriola (2007), Modeling metabolic reductive dechlorination in dense non-aqueous phase liquid source-zones. *Adv. Water Resour.*, *30*(6–7), 1547–1561, doi:10.1016/j.advwatres.2006.05.024

Conrad, S. H., J. L. Wilson, W. R. Mason, and W. J. Peplinski (1992), Visualization of residual organic liquid trapped in aquifers, *Water Resour. Res.*, *28*(2), 467–478.

Cooling, M. R., B. Khalfaoui, and D. M. T. Newsham (1992), Phase equilibria in very dilute mixtures of water and unsaturated chlorinated hydrocarbons and of water and benzene, *Fluid Phase Equilib.*, *81*(1–2), 217–229.

Cope, N., and J. B. Hughes (2001), Biologically-enhanced removal of PCE from NAPL source zones, *Environ. Sci. Technol.*, *35*, 2014–2021.

Crittenden, J. C., N. J. Hutzler, D. G. Geyer, J. L. Oravitz, and G. Friedman (1986), Transport of organic-compounds with saturated groundwater flow: Model development and parameter sensitivity, *Water Resour. Res.*, *22*(3), 271–284.

Fredenslund, A., R. L. Jones, and J. M. Prausnitz (1975), Group-contribution estimation of activity coefficients in nonideal liquid-mixtures, *AIChE J.*, *21*(6), 1086–1099.

Geller, J. T., and J. R. Hunt (1993), Mass-transfer from nonaqueous phase organic liquids in water-saturated porous media, *Water Resour. Res.*, *29*(4), 833–845.

Gmehling, J., P. Rasmussen, and A. Fredenslund (1982), Vapor-liquid-equilibria by UNIFAC group contribution: Revision and extension. 2. *Ind. Eng. Chem. Process Des. Dev.*, *21*, 118–127.

Hansen, H. K., P. Rasmussen, A. Fredenslund, M. Schiller, and J. Gmehling (1991), Vapor-liquid equilibria by UNIFAC group contribution. 5. Revision and extension, *Ind. Eng. Chem. Res.*, *30*(10), 2352–2355.

Hatfield, K., and T. B. Stauffer (1993), Transport in porous-media containing residual hydrocarbon. 1. Model, *J. Environ. Eng.*, *199*(3), 540–558.

Hayduk, W., and H. Laudie (1974), Prediction of diffusion coefficients for nonelectrolytes in dilute aqueous solutions. *AIChE J.*, *20*(3), 611–615.

Huang, J. C., D. Rothstein, and R. Madey (1984), Analytical solution for a first-order reaction in a packed bed with diffusion, *AIChE J.*, *30*(4), 660–662.

Imhoff, P. T., P. R. Jaffé, and G. F. Pinder (1994), An experimental study of complete dissolution of a nonaqueous phase liquid in saturated porous media, *Water Resour. Res.*, *30*(2), 307–320.

Interstate Technology and Regulatory Council (2008) *In Situ Bioremediation of Chlorinated Ethene: DNAPL Source Zones*, Interstate Technol. Regul. Counc., Washington, D. C.

Jin, M., M. Delshad, V. Dwarakanath, D. C. McKinney, G. A. Pope, K. Sepehrnoori, C. E. Tilburg, and R. E. Jackson (1995), Partitioning tracer test for detection, estimation and remediation performance assessment of subsurface nonaqueous phase liquids, *Water Resour. Res.*, *31*(5), 1201–1211.

Johns, M. L., and L. F. Gladden (1999), Magnetic resonance imaging study of the dissolution kinetics of octanol in porous media, *J. Colloid Interface Sci.*, *210*(2), 261–270.

Leij, F. J., N. Toride, and M. T. van Genuchten (1993), Analytical solutions for non-equilibrium solute transport in three-dimensional porous-media, *J. Hydrol.*, *151*(2–4), 193–228.

Li, P., G. Xiu, and A. E. Rodrigues (2003), Analytical breakthrough curves for inert core adsorbent with sorption kinetics, *AIChE J.*, *49*(11), 2974–2979.

Mayer, A. S., and C. T. Miller (1992), The influence of porous medium characteristics and measurement scale on pore-scale distributions of residual nonaqueous-phase liquids, *J. Contam. Hydrol.*, *11*, 189–213.

Miller, C. T., M. M. Poirier-McNeill, and A. S. Mayer (1990), Dissolution of trapped nonaqueous phase liquids: Mass transfer characteristics, *Water Resour. Res.*, *26*(11), 2783–2796.

Nkedi-Kizza, P., P. S. C. Rao, R. E. Jessup, and J. M. Davidson (1982), Ion exchange and diffusive mass transfer during miscible displacement through an aggregated oxisol, *Soil Sci. Soc. Am. J.*, *46*, 471–476.

Pellett, G. E. (1964), Longitudinal dispersion, intrafiber diffusion, and liquid phase mass transfer during flow through fiber beds, Ph.D. dissertation, Inst. of Paper Chem., Lawrence Coll., Appleton, Wisc.

Pennell, K. D., L. M. Abriola, and W. J. Weber (1993), Surfactant-enhanced solubilization of residual dodecane in soil columns. 1. Experimental investigation, *Environ. Sci. Technol.*, *27*(12), 2332–2340.

Porter, M. L., D. Wildenschild, G. Grant, and J. I. Gerhard (2010), Measurement and prediction of the relationship between capillary pressure, saturation, and interfacial area in a NAPL–water–glass bead system. *Water Resour. Res.*, *46*, W08512, doi:10.1029/2009WR007786.

Powers, S. E. (1992), Dissolution of nonaqueous phase liquids in saturated subsurface systems, Ph.D. dissertation, Dep. of Civ. and Environ. Eng., Univ. of Mich., Ann Arbor.

Powers, S. E., L. M. Abriola, and W. J. Weber Jr. (1992), An experimental investigation of nonaqueous phase liquid dissolution in saturated subsurface systems: Steady state mass transfer rates, *Water Resour. Res.*, *28*(10), 2691–2705.

Powers, S. E., L. M. Abriola, and W. J. Weber Jr. (1994a), An experimental investigation of nonaqueous phase liquid dissolution in saturated subsurface systems: Transient mass transfer rates, *Water Resour. Res.*, *30*(2), 321–332.

Powers, S. E., L. M. Abriola, J. S. Dunkin, and W. J. Weber Jr. (1994b), Phenomenological models for transient NAPL-water mass-transfer processes, *J. Contam. Hydrol.*, *16*(1), 1–33.

Ramsburg, C. A., and K. D. Pennell (2002), Density-modified displacement for dense nonaqueous phase liquid source-zone remediation: Density conversion using a partitioning alcohol, *Environ. Sci. Technol.*, *36*(9), 2082–2087, doi:10.1021/es0113571.

Ramsburg, C. A., C. E. Thornton, and J. A. Christ (2010), Degradation product partitioning in source zones containing chlorinated ethene DNAPL, *Environ. Sci. Technol.*, *44*(23), 9105–9111, doi:10.1021/es102536f.

Rao, P.S.C., D.E. Rolston, R. E. Jessup, and J. M. Davidson (1980), Solute transport in aggregated porous media: theoretical and experimental evaluation, *Soil Sci. Soc. Am. J.*, *44*(6), 1139–1146.

Rasmuson, A., and I. Neretnieks (1980), Exact solution of a model for diffusion in particles and longitudinal dispersion in packed-beds, *AIChE J.*, *26*(4), 686–690.

Rasmuson, A., and I. Neretnieks (1981), Migration of radionuclides in fissured rock: The influence of micropore diffusion and longitudinal dispersion, *J. Geophys. Res.*, *86*(B5), 3749–3758.

Schnaar, G., and M. L. Brusseau (2005), Pore-scale characterization of organic immiscible-liquid morphology in natural porous media using synchrotron X-ray microtomography, *Environ. Sci. Technol.*, *39*(21), 8403–8410, doi:10.1021/es058370.

Smith, J. M., and H. C. Van Ness (1987), *Introduction to Chemical Engineering Thermodynamics*, 4th ed., McGraw-Hill, New York.

Sørensen, J. M., T Magnussen, P. Rasmussen, and A. Fredenslund (1979), Liquid-liquid equilibrium data: Their retrieval, correlation and prediction, *Fluid Phase Equilib.*, *2*, 297–309.

Toride, N., F. J. Leij, and M. T. van Genuchten (1993), A comprehensive set of analytical solutions for nonequilibrium solute transport with 1st-order decay and zero-order production, *Water Resour. Res.*, *29*(7), 2167–2182.

Toride, N., F. J. Leij, and M. T. van Genuchten (1999), The CXTFIT code for estimating transport parameters from laboratory or field tracer experiments, Version 2.1, *U. S. Salinity Lab. Agric. Res. Serv. Rep. 137*, pp. 119, U.S. Dep. of Agric., Riverside, Calif.

van Genuchten, M. T. (1985), A general approach for modeling solute transport in structured soils, *Hydrogeol. of rocks of low permeability, Proc. Int. Assoc. Hydrogeol. Cong.*, *17*(2), 513–526.

van Genuchten, M. T., and W. J. Alves (1982), Analytical solutions of the one-dimensional convective-dispersive solute transport equation, *Tech. Bull. 1661*, 151 pp., U.S. Dep. of Agric., Washington, D. C.

van Genuchten, M. T., and R. J. Wagenet (1989), Two site/two region models for pesticide transport and degradation: theoretical development and analytical solutions. *Soil Sci. Soc. Am. J.*, *53*(5), 1303–1310.

van Genuchten, M. T., and P. J. Wierenga (1976), Mass-transfer studies in sorbing porous-media. 1. Analytical solutions, *Soil Sci. Soc. Am. J.*, *40*(4), 473–480.

van Genuchten, M. T., and P. J. Wierenga (1977), Mass-transfer studies in sorbing porous-media. 2. Experimental evaluation with tritium, *Soil Sci. Soc. Am.. J.*, *41*(2), 272–278.

van Genuchten, M. T., P. J. Wierenga, and G. A. O'Connor (1977), Mass transfer studies in sorbing porous media: III. Experimental evaluation with 2,4,5 T, *Soil Sci. Soc. Am. J.*, *41*(2), 278–285.

Weber, W. J., Jr., and F. A. DiGiano (1996), Process Dynamics in Environmental Systems, John Wiley, New York.

Willson, C. S., O. Pau, J. A. Pedit, and C. T. Miller (2000), Mass transfer rate limitation effects on partitioning tracer tests, *J. Contam. Hydrol.*, *45*(1–2), 79–97.

Yang, Y., and P. L. McCarty (2000), Biologically enhanced dissolution of tetrachloroethene DNAPL, *Environ. Sci. Technol.*, *34*(14), 2979–2984.

Yang, Y. and P. L. McCarty (2002), Comparison between donor substrates for biologically enhanced tetrachloroethene DNAPL dissolution, *Environ. Sci. Technol.*, *36*(15), 3400–3404, doi:10.1021/es011408e.

Yu, S., and L. Semprini (2009). Enhanced reductive dechlorination of PCE DNAPL with TBOS as a slow release electron donor. *J. Hazard. Mater.*, *167*(1–3), 97–104, doi:10.1016/j.jhazmat.2008.12.087.

A. Boroumand and C. A. Ramsburg, Department of Civil and Environmental Engineering, Tufts University, 200 College Ave., Rm. 113, Anderson Hall, Medford, MA 02155, USA. (andrew.ramsburg@tufts.edu)

J. A. Christ, Department of Civil and Environmental Engineering, USAF Academy, 2354 Fairchild Dr., Ste. 6J-159, Colorado Springs, CO 80840-6236, USA.

S. R. Douglas, Geosyntec Consultants, Bldg. 1-B, Ste. 205, 3131 Princeton Pike, Lawrenceville, NJ 08648, USA. (sdouglas@geosyntec.com)